Resistive or Capacitive Charge-Division Readout for Position-Sensitive Detectors

Alberto Pullia, Walter F. J. Müller, Ciro Boiano, and Roberto Bassini

***Abstract*—Two-point charge division is a typical technique for position measurements in linear multi electrode detectors (microstrips, multiwire proportional counters, silicon drift-detector arrays, and scintillators coupled to photodetectors). Only two preamplifiers, located at the right and the left ends of the detection array, are used, each of which receives a fraction of the charge produced by the ionizing event. Position is reconstructed comparing these charge fractions. In principle, either a resistive or a capacitive divider may be used to split the charge. The choice between such two different setups is not obvious. In fact, each of them shows advantages and disadvantages in terms of noise, signal propagation, and linearity. In this paper, we present a unified treatment for the capacitive and the resistive mechanisms of charge division that addresses the issues of this choice. As an example, the realistic setup of the multiwire position-sensitive proportional counter to be used in the TP-MUSIC III chamber of the ALADiN experiment at GSI is considered.**

***Index Terms*—Charge division readout, Position-sensitive detectors, posihon, measurements, .**

I. Introduction

TWO-POINT charge splitting is a measurement technique aimed at identifying the position of an ionizing event in linear multi-electrode detectors [microstrips, multiwire proportional counters (MWPC), silicon drift-detector arrays, scintillators coupled to segmented photodetectors] [1], [2]. Rather than using an electronic channel per electrode, it makes use of only two "virtual-earth preamplifiers" with their virtual earths connected to the right and the left ends of the electrode array. Each preamplifier receives a fraction of the total charge produced by the event. The relative position x of the event along the array depends on these charge fractions, or

$$\chi = \frac{x}{x_T} = \frac{Q_R}{Q_R + Q'_L} \tag{1}$$

where x_T is the total length of the array, Q_R is the charge collected at the right end point, Q_L is the charge collected at the left-end point, and the total charge $Q_R + Q_L$ is used as a normalization factor. Both a resistive and a capacitive divider may be used to split the charge into fractions Q_L and Q_R, as is shown in the examples of Fig. 1. Each of these setups shows advantages and disadvantages in terms of noise, signal propagation, and linearity, which depend on the constraints dictated by the detection system

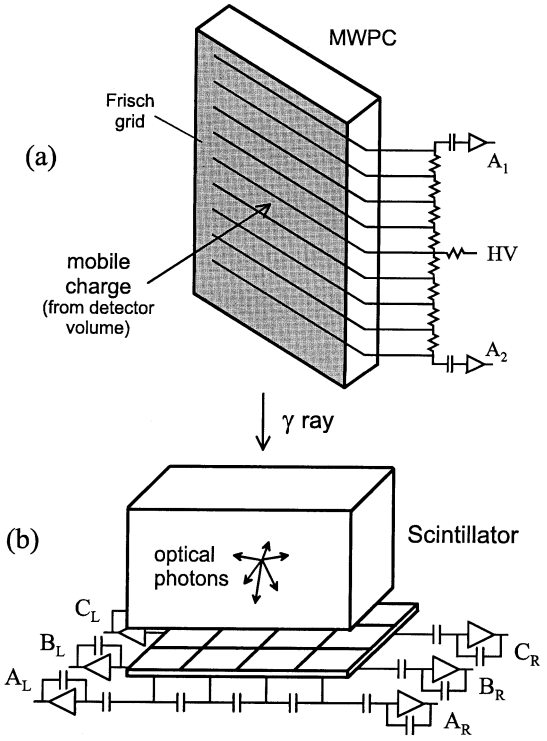

Fig. 1. Charge division in (a) a multiwire proportional counter and (b) a matrix of photodetectors coupled to a scintillator.

(capacitance and number of electrodes, required processing time, and necessity of decoupling capacitors). In this paper, a unified treatment for the capacitive and resistive mechanisms of the charge division is presented. The signal shape as well as the obtainable position resolution are derived versus a suitable pattern of detector–processor parameters. It is found that the capacitive charge-division yields a higher resolution unless very short processing times are required. As an example, the physical parameters of the MWPC of the TP-MUSIC III chamber installed at GSI are considered. This MWPC consists of a plane of anode wires (diameter $=$ 20 μm, 5-mm spacing) shielded from the detector volume by a Frisch grid located 5 mm away. The Frisch grid acts as a gate that can be "closed" when necessary, so as to prevent the slow positive ions produced in the multiplication volume from back scattering into the detector volume. The electrons traverse the region between the Frisch grid and the anode wires in 80–100 ns. The maximum time width of the charge cloud trespassing the Frisch grid, caused by thermal diffusion or by inclined trajectories of the primary ionizing particles, ranges between 20 and 150 ns, which sets a minimum for the processing time at about 200 ns. The shortest processing time is required in this application to maximize the resolving time in case of double or multiple hits in the detector volume.

Manuscript received November 22, 2001; revised July 23, 2002. This work was supported by INFN and MIUR, Milano, Italy, and by GSI, Darmstadt, Germany.

A. Pullia is with the Department of Physics, University of Milan, 20133 Milano, Italy, and is also with INFN, 20133 Milano, Italy (e-mail: alberto.pullia@mi.infn.it).

W. F. J. Müller is with GSI, D-64291 Darmstadt, Germany.

C. Boiano and R. Bassini are with INFN, 20133 Milano, Italy.

Digital Object Identifier 10.1109/TNS.2002.805521

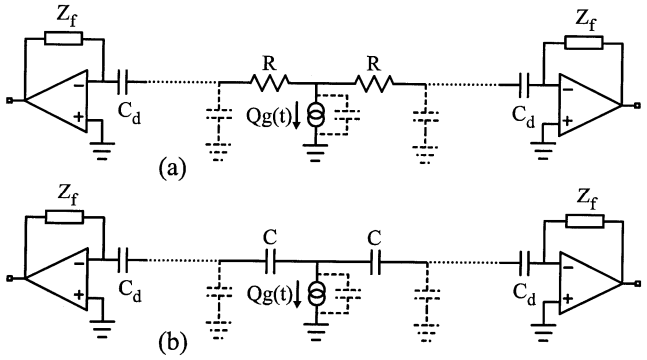

Fig. 2. Two-point measurement by means of (a) resistive divider (the stray capacitances in parallel to resistors R are neglected) and (b) capacitive divider. The resistors R or capacitances C connect all detection elements to each other. Each detection element has a capacitive impedance to ground (capacitances in dashed line). The current signal delivered by the detector is $Qg(t)$, where Q is the charge, and unit-area function $g(t)$ models the charge–collection mechanism. Decoupling capacitances C_d are also shown.

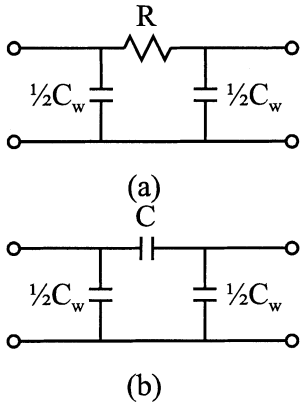

Fig. 3. Elementary cells by which the charge-division line may be modeled. C_w is the electrode (wire) capacitance. Elementary device for charge division is (a) a resistor R or (b) a capacitance C.

An entirely different approach is based on terminating both ends of the charge-splitting line into the line characteristic impedance and use propagation times to derive the position. However, such an approach is beyond the scope of this paper.

II. Signal Propagation and Nonlinearities

An electrical model of the charge-division line is shown in Fig. 2, where the electrode capacitances are drawn in dashed line. The signal is modeled as a short current pulse $Qg(t)$, where Q is the collected charge and $g(t)$ is a unit-area shape factor depending on the charge–collection mechanism. Decoupling capacitors C_d are also shown, whereas the high-value resistors used to bias the detector have been neglected. We want to calculate the current flowing into the virtual earths of the two far-end amplifiers as a function of the position of firing electrode. To do this, let us model the network as the cascade of identical symmetrical π-type cells of the type of those of Fig. 3, connected as shown in Fig. 4. Impedances Z_T terminating the line at both ends model the decoupling capacitors and the virtual earths. Virtual earths act as electronically cooled damping resistors [1], typically a few tens of ohms. These low-value resistors can be neglected in first approximation. C_w is the capacitance of the electrodes, and R or C are the charge-splitting devices. Z_0 is the characteristic impedance of the cell, or the impedance seen at the input of a semi-infinite line ($\Re$) of identical cells [3]. Parameter k is the so-called transduction exponent of the cell, defined as the natural logarithm of the input-to-output voltage ratio of each cell of such a line ($\Re$) [3]. It can be shown that any symmetric cell is fully characterized by parameters Z_0 and k. After some calculations, shown in Appendix I-A and I-B, we derive

$$Z_0 = \begin{cases} \sqrt{\dfrac{R}{sC_w(1+(1/4)sRC_w)}} \\ \dfrac{1}{s\sqrt{CC_w+(1/4)C_w^2}} \end{cases}$$

$$k = \begin{cases} \cosh^{-1}(1+(1/2)sRC_w) \\ \cosh^{-1}\left(1+(1/2)\dfrac{C_w}{C}\right) \end{cases} \tag{2}$$

for cells of Fig. 3(a) [first and third row of (2)] and (b) [second and fourth row of (2)]. s is the independent variable in the Laplace domain. In Fig. 4, Z_1 and Z_2 are the impedances seen at the right/left side of the firing electrode. As is shown in Appendix I-C

$$Z_i = Z_0 \frac{Z_T \cosh n_i k + Z_0 \sinh n_i k}{Z_T \sinh n_i k + Z_0 \cosh n_i k} \tag{3}$$

where $i = 1, 2$. n_1 and n_2 are the cells located at the right/left side of the firing electrode. The signal current I_0 is split by current divider Z_1–Z_2 and flows thereafter through the line toward the far-end amplifiers. By using the current divider formula and (39) of Appendix I-C, it is found that

$$I_{n1} = \frac{\cosh n_2 k + \frac{Z_0}{Z_T}\sinh n_2 k}{\left(\frac{Z_T}{Z_0}+\frac{Z_0}{Z_T}\right)\sinh nk + 2\cosh nk} I_0 \tag{4}$$

where indexes 1 and 2 can be swapped and $n = n_1 + n_2$. If no coupling capacitor is used, Z_T vanishes and (3) and (4) become much simpler, namely

$$Z_i = Z_0 \tanh n_i k, \tag{5}$$

$$I_{n1} = \frac{\sinh n_2 k}{\sinh nk} I_0. \tag{6}$$

Equations (4) and (6) show in the Laplace domain the propagation of the current signal from the firing electrode to the right-end amplifier. Equations (4) and (6) hold namely when the line is terminated into the amplifier virtual earth through impedance Z_r or a short-circuit connection. Approximating $g(t)$ as a delta-like impulse, I_0 becomes the Laplace transform of function $Q\delta(t)$, or $I_0 = L(Q\delta(t)) = Q$. Inverse Laplace transform of (4) or (6) yields the current flowing into the amplifier virtual earth, which is clearly a function of n_2, or the position of the firing electrode.

A. Resistive Divider

For the case of a resistive divider, the first row of (2) holds. We search the time-domain counterparts of (4) and of (6) with $Z_T = 1/sC_d$ and $I_0 = L(Q\delta(t)) = Q$. To this purpose, it is necessary to calculate the roots of the denominator of (4) and

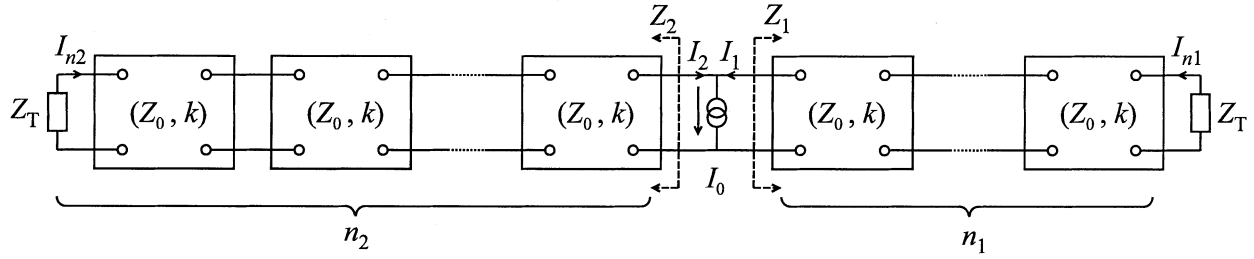

Fig. 4. Equivalent circuit of a charge-splitting line. Any cell models the charge-division element (a resistor or a capacitor) and the electrode impedance. The line is terminated into virtual earths of far-end amplifiers through coupling capacitors as modeled by impedances Z_T.

(6), or the poles of the network. After some calculations, it turns out that the denominator of (4) may be rewritten as

$$\left(s\,\frac{\tau_w^2+4\tau_d^2}{4\tau_d}+\frac{C_w}{C_d}\right)\prod_{h=1}^{n-1}\left(s+\frac{4}{\tau_w}\sin^2\frac{h\pi}{2n}\right)+\tau_w\prod_{h=0}^{n-1}\left(s+\frac{4}{\tau_w}\sin^2\frac{2h+1}{4n}\pi\right) \quad (7)$$

where $\tau_d = RC_d$ and $\tau_w = RC_w$. Apparently, this polynomial is the sum of two polynomials, each with n known real roots, and it therefore has n roots. Furthermore, the roots of the overall polynomial are distinct and can be easily derived numerically. Similarly, the denominator of (6) may be rewritten as

$$\prod_{h=1}^{n-1}\left(s+\frac{4}{\tau_w}\sin^2\frac{h\pi}{2n}\right) \quad (8)$$

which apparently has $n-1$ distinct real roots. Whenever all poles are distinct, the inverse Laplace transform can be calculated using the well-known relationship

$$L^{-1}\left\{\frac{N(s)}{D(s)}\right\}=\sum_r\frac{N(\alpha_r)}{D'(\alpha_r)}\,e^{\alpha_r t} \quad (9)$$

where L^{-1} is inverse Laplace transform, α_r is the rth root of $D(s)$, the prime stands for derivative versus s, and t is time. We can use (9) to translate (4) (with $Z_T = 1/sC_d$) in the time domain, being α_r the roots of (7). Similarly, we can switch (6) in the time domain, obtaining, in this case, exactly

$$i_{n1}(t)=\frac{2Q}{n\tau_w}\sum_{r=1}^{n-1}(-1)^{r+1}\sin\frac{n_2 r\pi}{n}\cdot\sin\frac{r\pi}{n}\,e^{-(4t/\tau_w)\sin^2(r\pi/n)}. \quad (10)$$

Equation (10) gives explicitly the current flowing into the virtual earth of the far-end amplifier when no decoupling capacitors are used, as a function of the position (dictated by n_2) of firing electrode. In Figs. 5–7, the integral of $i_{n1}(t)$, or the transmitted charge, is shown as normalized to the total collected charge Q for realistic values of the parameters. Note the effect of the decoupling capacitances in Figs. 6 and 7. The waveforms converge to a common final value of about one-half of the total collected charge. This is rather intuitive: the collected charge cannot be eventually transmitted out of the resistor chain due to the decoupling capacitances that act as a barrier at low frequency. The charge will rather get redistributed on the large-value decoupling capacitors. This yields $(1/2)Q$ on each of the

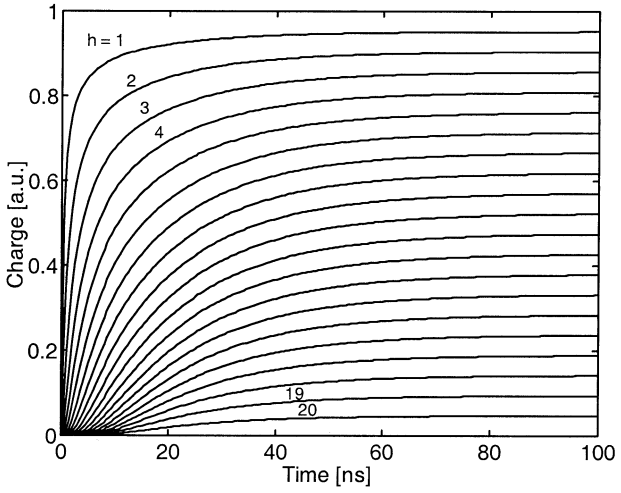

Fig. 5. Charge signal reaching one far-end amplifier in a proportional counter with 20 wires. Index h is the position of the firing wire, in ascending order as the electrode gets further from the amplifier. $R_{\rm tot} = 1.8$ kΩ, or $R = 90\ \Omega$. $C_w = 4.5$ pF. No decoupling capacitors are used. The waveforms stabilize after 100 ns.

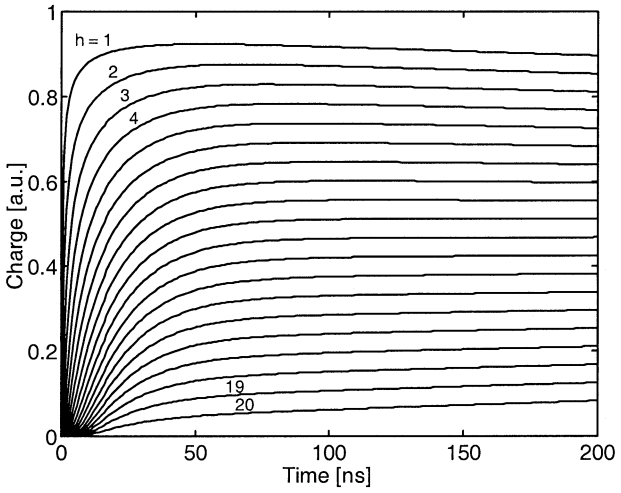

Fig. 6. Same as in Fig. 5 (20 electrodes, $R = 90\ \Omega$. $C_w = 4.5$ pF) but with decoupling capacitors of 2.2 nF. Note the effect of decoupling capacitors; the waveforms never reach stable values.

decoupling capacitances (assuming them equal to each other). It is worth pointing out that such a charge will be drained away in the long term by the high-value resistors used to bias the electrodes. Figs. 6 and 7 show clearly that if decoupling capacitors are used, linearity will eventually depend on the shaping time constant. To address this problem sufficiently, large decoupling

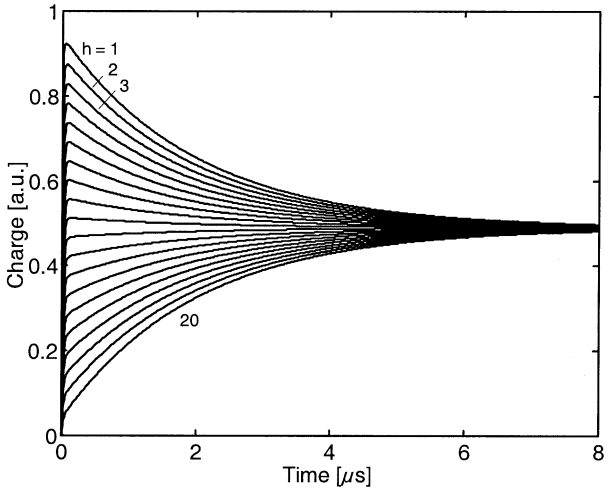

Fig. 7. Same as in Fig. 6, but on an expanded time scale. It can be seen that the waveforms decay exponentially, converging to a common final level of about one-half of the total collected charge Q (waveforms are normalized to Q in the figure). The time constant is dictated by the overall resistance of the divider and the series of the two decoupling capacitances, or 1.8 kΩ $\times$ 1.1 nF $= 2$ μs.

capacitances are to be used, in such a way that the time constant of the charge redistribution process, or

$$(nR)\left(\tfrac{1}{2}\,C_d\right) \tag{11}$$

is greater than the used shaping time. Alternatively, a differentiator followed by a baseline restorer could be used to clip the slow tail caused by the decoupling capacitors.

The principal advantage of a resistive divider is a good linearity of the fraction (1) versus position relationship. In fact, at low frequency, the electrode capacitances C_w behave as open-circuit connections and linearity is only limited by the accuracy of the divider resistors. This can be seen in Fig. 5. Aafter $\sim$100 ns linearly distributed saturation values are reached. From a mathematical standpoint, this can be seen in (6), where $I_0 = Q$. If s vanishes, which corresponds to pushing t to infinity, then $k \rightarrow 0$ in (2), and (6) converges exactly to $(n_2/n)Q$. However, capacitances C_w along with resistors R introduce phase shifts at high frequencies along the signal path, which yield a transient (noticeable for $t < 50$ ns) and propagation delays (noticeable for $t < 15$ ns), which get larger as the firing wire is further from the amplifier. To minimize such effects, the resistor values should be chosen relatively low (90 Ω in the shown examples). An empirical rule to determine the maximum transient duration (τ_0) is

$$\tau_0 \approx (nR)\left(\tfrac{1}{2}\,nC_w\right) \tag{12}$$

which also permits us to derive R as a function of the transient duration. As is shown in Appendix II-A, (12) can be seen as the time constant of the line impedance as approximated at suitably low frequencies with a resistance (nR) and a capacitance ($(1/2)nC_w$) connected in parallel. Resistance nR is the series of n elementary resistors, capacitance $(1/2)nC_w$ is one-half of the parallel connection of all electrode capacitances C_w. Factor one-half arises because a voltage V supplied at one end of the line degrades to zero approaching the far end of the line and

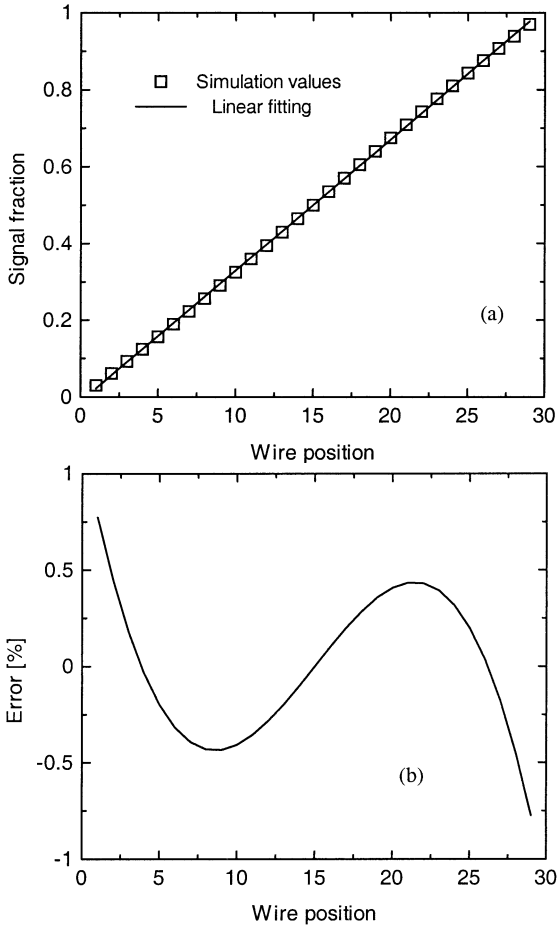

Fig. 8. Charge division with a capacitive-divider setup for a multiwire proportional counter. Fraction (1) is reported versus the wire position while considering 29 wires. Wire capacitance is 0.8 pF. The capacitances C of the divider as well as C_d are of 1.1 nF. The nonlinearity is predicted to be $<$1%.

therefore the total charge stored on capacitances C_w is one-half of $V \times nC_w$. Low-value resistors should be used to make the transient (12) fast. The price to be paid for low-value resistors is a large amount of parallel current noise, as described in Section III.

B. Capacitive Divider

For the case of a capacitive divider, the second and fourth row of (2) holds. Note that in this case, k is a constant and Z_0 is the impedance of a capacitance. Assume again $I_0 = Q$. With these assumptions, (4) with $Z_T = 1/sC_d$ shows no dependence on s, and in consequence, its time-domain counterpart is a delta-like function. This is not surprising. The line is a passive circuit made by capacitances only and thus, has no bandwidth limitation. This is an advantage against the resistive-divider setup. In fact, the transmitted charge, or the integral of $i_{n1}(t)$, is a clean-step function. However, the dependence of fraction (1) on position is nonlinear. In fact, capacitances C_w sink small amounts of charge away from the main capacitive divider, which affects the linearity of the divider itself. In Fig. 8, the loss of linearity as derived from (6) is shown for realistic values of the parameters. To minimize this nonlinearity, relatively large capacitances should

be used in the divider. An empirical rule for such dimensioning is

$$\frac{C}{n} > n\,\frac{C_w}{2} \tag{13}$$

in which a comparison is made between approximations of the charge stored onto the series of n capacitances C and that sunk away by capacitances C_w. The sum of the capacitances shown in (13) is a good approximation of the total line capacitance as is shown in Appendix II-B. If (13) is verified, linearity will be mainly limited by the accuracy of the divider capacitors. Note that high-voltage capacitors should be used because typically thousands of volts are provided to bias the electrodes: if an electrode breaks down, a fast-rising charge would be induced on the nearby capacitances and they could get damaged.

Advantages of a capacitive divider include a fast response and a low noise, as will be shown in Section III.

III. Noise of Position Figure

The complex impedance Z_n of the charge divider is the input load of the amplifiers, and it is given by (46) and (48) of Appendix II-A and II-B, i.e.,

$$Y_n = \frac{1}{Z_n} \approx s\frac{1}{2}\,nC_w + Y \tag{14}$$

where from now on $s = j\omega$, and

$$Y = \begin{cases} \dfrac{1}{nR} & \text{(resistive divider)} \\ s\,\dfrac{C}{n} & \text{(capacitive divider).} \end{cases} \tag{15}$$

Y_n has the form of a capacitance and a resistor in parallel (resistive divider) or of two capacitances in parallel (capacitive divider). Y represents the obvious component of Y_n interconnecting the virtual earths of the two preamplifiers. The other component is associated with the electrode capacitances and can be visualized as a leakage path to ground. The Johnson noise (bilateral) associated with Y_n is

$$\begin{aligned} \overline{i^2} &= 2KT\mathrm{Re}\{Y_n\}\delta f \\ &= \begin{cases} \dfrac{2KT}{nR}\,\delta f = b_0\delta f & \text{(resistive divider)} \\ 0 & \text{(capacitive divider)} \end{cases} \end{aligned} \tag{16}$$

where $\mathrm{Re}\{Y_n\}$ denotes the real component of Y_n, K is the Boltzmann constant, T is absolute temperature, and the other symbols are obvious. The principal noise sources at the right-end amplifier input are shown in Fig. 9, where noise injection from the opposite-end amplifier through path Y is apparent. In the left-end amplifier, e_1 and i_1 must be replaced with e_2 and i_2 and e_2 with e_1. The following relations hold for the series and parallel noises (bilateral):

$$\begin{aligned} \overline{e_1^2} &= \overline{e_2^2} = 2KTR_S\delta f = a\delta f \\ \overline{i_1^2} &= \overline{i_2^2} = \left(\frac{2KT}{R_F} + qI_L\right)\delta f = b\delta f. \end{aligned} \tag{17}$$

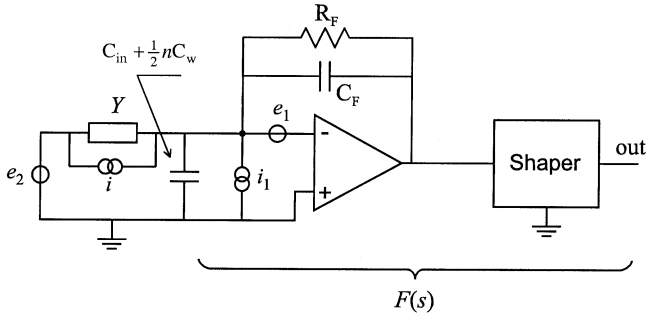

Fig. 9. Equivalent circuit of right-end amplifier and shaper useful for noise calculations. Swap indexes 1 and 2 of noise sources to get the equivalent circuit of left-end amplifier.

For an FET, $R_S = \alpha/g_m$, where g_m is its transconductance and α is a constant factor ranging from 0.5 to 1 [4]; and for a BJT, $R_S = 1/2g_m + R_{bb'}$, where $R_{bb'}$ is the base spreading resistor, R_F is the feedback resistor of the amplifier, q is the electronic charge, and I_L is the leakage current of the input transistor. In semiconductor detectors, I_L should include an effective current obtained by summing all electrode's leakage currents, each weighted linearly from 0 to 1 as the electrode position gets closer to the amplifier. Other nonwhite-noise contributions [5] have been neglected. C_{in} and C_F are the input and feedback capacitances of the amplifier. Note that the instantaneous Johnson-noise current (16) entering the right-end amplifier and that entering the left-end amplifier are anticorrelated. The series-noise cross talk through path Y introduces an additional correlation between the amplifiers' noises. These noise correlations must be taken into account in deriving the total noise of the position figure (1). Fig. 10(a) and (b) shows the equivalent circuits for noise analysis of the right- and the left-end amplifiers, where conventional signs are used for the instantaneous noise voltages and currents to highlight their correlations. Appendix III shows how these equivalent circuits are derived. $F(s)$ is the Laplace transform of the impulse response $F(t)$ of the amplifier-shaper chain normalized to its maximum value. Note that with such a normalization a current, $Q\delta(t)$ fed into the amplifier's virtual earth causes a signal at the shaper output with height Q.

Noise of position figure (1) in a bandwidth from f to $f + \delta f$ is given by the error propagation law or by

$$\begin{aligned} \overline{|d\chi|^2} = \left|\frac{\partial\chi}{\partial Q_R}\right|^2 \overline{|dQ_R|^2} + \left|\frac{\partial\chi}{\partial Q_L}\right|^2 \overline{|dQ_L|^2} \\ +2\mathrm{Re}\left\{\frac{\partial\chi}{\partial Q_R}\,\frac{\partial\chi^*}{\partial Q_L}\,\overline{dQ_R dQ_R^*}\right\} \end{aligned} \tag{18}$$

where the star stands for complex conjugate, and

$$\begin{aligned} Q_R &= h_2 Q \approx \frac{n_2}{n}\,Q \\ Q_L &= h_1 Q \approx \frac{n_1}{n}\,Q. \end{aligned} \tag{19}$$

Equations (18), (1), and (19) yield

$$\overline{|d\chi|^2} = \frac{h_1^2}{Q^2}\,\overline{|dQ_R|^2} + \frac{h_2^2}{Q^2}\,\overline{|dQ_L|^2} - 2\frac{h_1 h_2}{Q^2}\,\mathrm{Re}\left\{\overline{dQ_R dQ_R^*}\right\}. \tag{20}$$

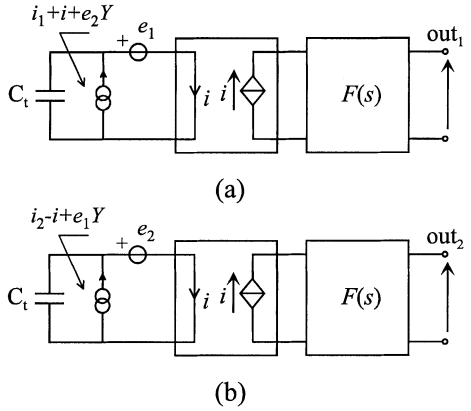

Fig. 10. Equivalent circuits of (a) right-end and (b) left-end amplifiers and shapers for noise calculations. A conventional direction is indicated for the instantaneous noise currents and voltages to highlight the correlations.

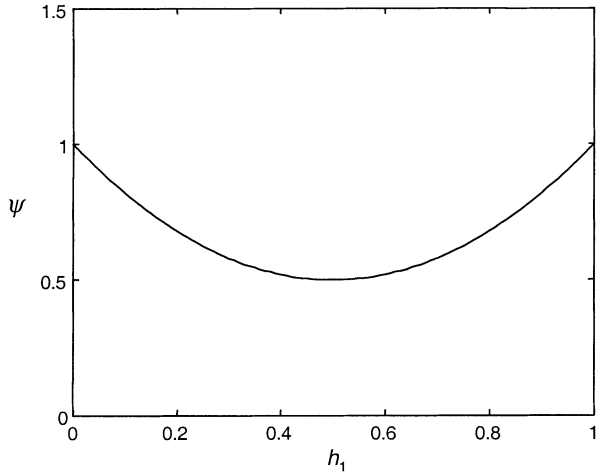

Fig. 11. Factor ψ versus $h_1 = n_1/n$. ψ ranges from 0.5 to 1 depending on the position of charge injection (from the middle of the array to the end points).

dQ_R and dQ_L are obtained from the equivalent circuits of Fig. 10, observing that the shaper output is read as an input-referred charge with the used normalization of $F(s)$

$$\begin{aligned} dQ_R &= i_1F(s) + iF(s) - e_1sC_tF(s) + e_2YF(s) \\ dQ_L &= i_2F(s) - iF(s) - e_2sC_tF(s) + e_1YF(s) \end{aligned} \quad (21)$$

where e_1, e_2, i_1, and i_2 are the instantaneous noise voltages and currents, and C_t is the sum of all capacitances connected to the amplifier input, including the capacitive component of Y

$$C_t = \begin{cases} C_{\text{in}} + C_F + \frac{1}{2}\,nC_w & (\text{resistive divider}) \\ C_{\text{in}} + C_F + \dfrac{1}{2}\,nC_w + \dfrac{C}{n} & (\text{capacitive divider}) \end{cases} \quad (22)$$

and so from (21)

$$\begin{aligned} \overline{|dQ_R|^2} &= \left(\overline{i_1^2} + \overline{i^2} + \overline{e_2^2}|Y|^2 + \overline{e_1^2}|sC_t|^2\right)|F(s)|^2 \\ \overline{|dQ_L|^2} &= \left(\overline{i_2^2} + \overline{i^2} + \overline{e_1^2}|Y|^2 + \overline{e_2^2}|sC_t|^2\right)|F(s)|^2 \\ \text{Re}\left\{\overline{dQ_R dQ_L^*}\right\} &= -\left[\overline{i^2} + \left(\overline{e_1^2} + \overline{e_2^2}\right)C_t\text{Re}\{sY^*\}\right]|F(s)|^2. \end{aligned} \quad (23)$$

In (23), the mean-squared voltages and currents are given by (16) and (17), Y is given by (15), and C_t by (22). Putting (23) in (20) and integrating over all values of f (from $-\infty$ to ∞), one obtains the variance σ_χ^2 of the position figure. Frequency dependence of (23) is dictated by factors $|F(j\omega)|^2$ or $\omega^2|F(j\omega)|^2$. The integral of such factors over the frequency is often translated in the time domain thanks to Parseval's theorem [6], [7] or to

$$\begin{aligned} \int_{-\infty}^{\infty} \omega^2|F(j\omega)|^2\,df &= \int_{-\infty}^{\infty} |F'(t)|^2\,dt = \frac{A}{T_P} \\ \int_{-\infty}^{\infty} |F(j\omega)|^2\,df &= \int_{-\infty}^{\infty} |F(t)|^2\,dt = BT_P \end{aligned} \quad (24)$$

where the prime stands for time derivative. T_P is the "time width parameter" of $F(t)$ or the "processing time" and A, B are nondimensional form factors depending on the shape of $F(t)$ and not on its time scale. Numerical values of A, B are listed for most cases in [8].

1) Case of Resistive Divider: Putting (23) with $Y = 1/nR$ in (20) and integrating over f with the help of (24), we thus obtain

$$\sigma_{\chi R}^2 = \frac{1}{Q^2}\left[\psi aC_{iR}^2\,\frac{A}{T_P} + (\psi b + b_0)BT_P\right] \quad (25)$$

where second index "R" denotes the resistive-divider case and $\psi = h_1^2 + h_2^2$ is a factor depending on the position of charge injection. Taking into account that (19) yields $h_1 + h_2 = 1$, one obtains $\psi = 2h_1^2 - 2h_1 + 1$. ψ is plotted versus h_1 in Fig. 11. It is worth noting that the dependence of (25) on ψ tends to vanish if the noise component b_0BT_P brought about by the resistive divider [see (16)] dominates over the others. This is rather intuitive: in this case, the noises seen at the output of the amplifiers are anticorrelated, and the noise of the sum is much lower than the noise of individual ends. Therefore, the error in the position figure (1) is dictated by the noise of one amplifier only, and it is thus independent of the location of the charge injection.

2) Case of Capacitive Divider: Putting (23) with $Y = sC/n$ in (20) and integrating over f with the help of (24), we obtain

$$\sigma_{\chi C}^2 = \frac{1}{Q^2}\left[\left(\psi + \frac{2-\psi}{n^2}\,\frac{C^2}{C_{tC}^2}\right)aC_{tC}^2\,\frac{A}{T_P} + \psi bBT_P\right] \quad (26)$$

where second index "C" denotes the capacitive-divider case. It is worth noting that the dependence of (26) on ψ tends again to vanish if C_{tC} is dominated by the capacitive divider, i.e., $C_{tC} \approx C/n$, and the series-noise component aC_{tC}^2A/T_P dominates. In this case, the cross talk between series noises makes the noises at the preamplifiers' outputs again anticorrelated, so that the noise of the sum is much lower than the noise of individual ends. Therefore, the error in the position figure (1) is dictated by the noise of one amplifier only and is thus independent of the location of the charge injection.

A comparison between resistive- and capacitive-divider setups translates into a comparison of the variances (25) and (26). The ratio between variances (26) and (25) is

$$r_{CR}^2 = \frac{\sigma_{\chi C}^2}{\sigma_{\chi R}^2} = \frac{\left(\psi + \frac{2-\psi}{n^2}\frac{C^2}{C_{tC}^2}\right) aC_{tC}^2 \frac{A}{T_P} + \psi b B T_P}{\psi a C_{tR}^2 \frac{A}{T_P} + (\psi b + b_0) B T_P} \quad (27)$$

which apparently depends on the processing time T_P. The resistive divider enhances the parallel noise (current noise of resistor nR) and the capacitive divider enhances the series noise (capacitance C/n enhances the total input capacitance C_{tC}). We so expect that the resistive divider has a better performance at short processing times and the opposite for the capacitive divider. However, a resistive setup with nR in the kohm range typically enhances the parallel-noise contribution by several orders of magnitudes with respect to capacitive setups, whereas a capacitive setup with C/n ranging from 50 to 500 pF typically increases the series-noise contribution by one order of magnitude with respect to resistive setups. We thus expect that in most cases, capacitive-charge division yields a higher resolution than does resistive division at the optimum processing times.

As an example, consider an MWPC of the type of that of Fig. 1(a) with 20 wires having $C_w = 4.5$ pF ($1/2nC_w = 45$ pF), and two possible dividers: the first made by 20 resistors of 90 Ω each ($nR = 1.8$ kΩ) and the second made by 20 capacitances of 4.4 nF ($C/n = 220$ pF) each. For both cases, the amplifier's input transistor has a capacitance $C_{\rm in} = 10$ pF and a transconductance $g_m = 10$ mS. I_L is assumed 0.5 nA and a symmetrical trapezoidal shaper amplifier with a flattop to base ratio of 1/3 is used ($A = 2$, $B = 1.67$). In Fig. 12, curve (1), $r_{\rm CR}^2$ is shown where the aforementioned parameters are used, $\psi = 1$ and the "processing time" is the width of the sloped edge of the trapezoid. Larger-than-unity values on the y-axis indicate convenience for resistive against capacitive divider and vice versa. Curve (2) has been obtained by increasing R proportionally to the processing time. In fact, the divider's resistance is a tradeoff between the transient time of the RC_w line and the parallel noise. If R is proportional to the processing time, the transient time will be always an acceptable fraction of the processing time and parallel noise will be not as high at longer processing times. Curves (1) and (2) do not change noticeably by varying ψ in the 0.5–1 range. It can be seen that for very fast processing times, shorter than ≈200 ns in the considered case, the resistive divider may yield a lower noise. At a processing time of 1 μs, however, the capacitive divider yields one-to-two orders of magnitude of lower noise.

It is worth pointing out that with an array of photodetectors coupled to a scintillator, the charge–collection mechanism would be in the microsecond range, and therefore, the noise analysis should be made at much longer processing times than in Fig. 12. In this case, a capacitive-divider setup would be more adequate.

A very simple system consisting of a discrete network of resistors and capacitors, custom-made charge amplifiers, and quasi-Gaussian shaper amplifiers has been arranged to check the shown theory. The observed signals and noise have been found in good agreement with (10), (25), and (26).

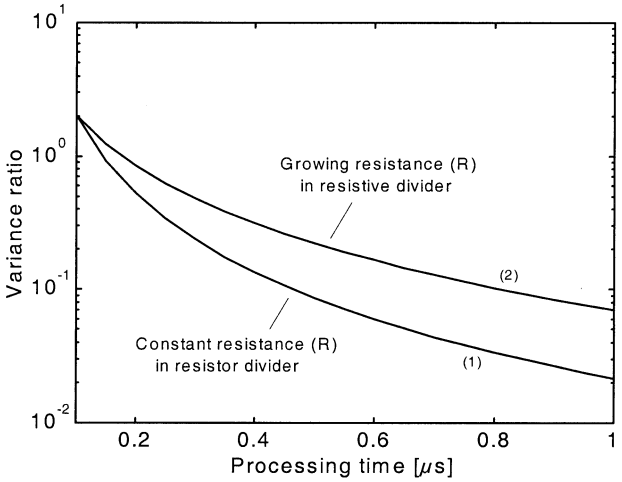

Fig. 12. Ratio of the variances of the position estimate for capacitive- and resistive-divider setups in a 20 wire ($C_w = 4.5$ pF) MWPC with Frisch grid. Parameters: $g_m = 10$ mS, $C_{\rm in} = 10$ pF. $C_F = 10$ pF. Capacitive divider: $C_{tC} = 285$ pF, $R_F = 50$ MΩ, $I_L = 0.5$ nA. Resistive divider: $C_{tR} = 65$ pF, $nR = 1.8$ kΩ, $R_F = 6$ kΩ, $I_L = 0.5$ nA.

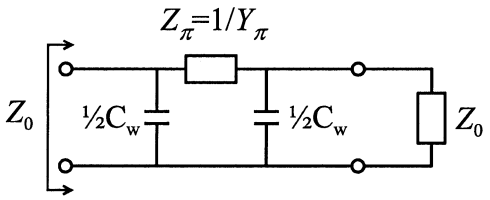

Fig. 13. Equivalent circuit for calculation of the characteristic impedance.

A different position figure or

$$\frac{Q_R - Q_L}{Q_R + Q_L} \quad (28)$$

is sometimes used rather than (1). Equation (28) ranges from -1 to 1 rather than from 0 to 1; thus, the signal swing gets doubled. However, the squared noise of such a figure, as obtained with the same procedure used to derive (25) and (26), is found to be four times as large. Therefore, (28) has the same SNR as (1). The shown analysis holds for both of them.

IV. Conclusion

The principal advantage of a resistive divider is the potentially good linearity of position figure versus position relationship. The price to be paid is a large amount of parallel noise. Such noise contribution decreases as the processing time is decreased. However, the processing time should be greater than the time transient due to phase shifts in the RC_w line and the intrinsic signal width caused by the charge-collection mechanism.

The principal advantages of a capacitive divider, instead, are a fast response and a low noise. However, the dependence of position figure versus position in this case is nonlinear. To minimize such nonlinearity, large-value capacitances should be used in the divider. However, these capacitances cannot be chosen too large because the series noise of the preamplifier is enhanced as the input capacitance is increased. A correct dimensioning of the divider capacitance appears as a tradeoff between nonlinearity and noise.

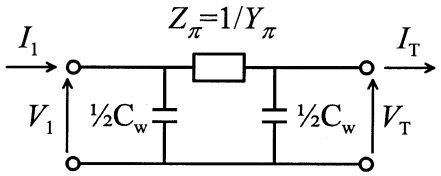

Fig. 14. Elementary π-type symmetric cell.

A unified method to derive the waveforms and the noise of the two configurations has been presented and discussed, and indications for a correct dimensioning of the setups have been shown. A possible development of the method consists of including $1/f$- and Lorentzian-noise components in the amplifiers' series noise.

Appendix I

A. Calculation of Characteristic Impedance Z_0

Z_0 is the input impedance of a semi-infinite line of identical cells. Let us connect a semi-infinite line of cells, as modeled by Z_0, to the output of an individual cell of the same type, as shown in Fig. 13.

The input impedance of such cell is again Z_0. By calculating it on the circuit of Fig. 13, we obtain the following identity (called $Y_0 = 1/Z_0$):

$$Y_0 = \frac{1}{2}\,sC_w + \frac{Y_\pi\left(Y_0 + \frac{1}{2}\,sC_w\right)}{Y_\pi + Y_0 + \frac{1}{2}\,sC_w}. \tag{29}$$

Solving (29) for Y_0, we obtain

$$Y_0^2 = sC_w\left(Y_\pi + \tfrac{1}{4}\,sC_w\right). \tag{30}$$

Putting $Y_\pi 1/R$ or $Y_\pi sC$ in (30) yields the first column of (2).

B. Calculation of Transduction Exponent k

Connect a voltage source $V_{\rm in}$ to the input of the cell of Fig. 13. Let us calculate the output voltage of this cell

$$V_{\rm out} = \frac{Y_\pi}{Y_\pi + Y_0 + \frac{1}{2}\,sC_w}\,V_{\rm in}. \tag{31}$$

Using Y_0 as given by (30) in (31), we find

$$\frac{V_{\rm in}}{V_{out}} = 1 + \frac{sC_w}{2Y_\pi} + \sqrt{\left(1 + \frac{sC_w}{2Y_\pi}\right)^2 - 1} \tag{32}$$

and hence

$$k = \ln\left(\frac{V_{\rm in}}{V_{out}}\right) = \cosh^{-1}\left(1 + \frac{sC_w}{2Y_\pi}\right). \tag{33}$$

Putting $Y_\pi 1/R$ or $Y_\pi sC$ in (33) yields the second column of (2).

C. Equations for the Series Connection of n Cells

Consider the cell of Fig. 14. The relations

$$\begin{cases} V_1 = V_T\left(1 + \frac{1}{2}\,sZ_\pi C_w\right) + I_T Z_\pi \\ I_1 = V_T\left(\frac{1}{4}\,s^2 Z_\pi C_w^2 + sC_w\right) + I_T\left(1 + \frac{1}{2}\,sZ_\pi C_w\right) \end{cases} \tag{34}$$

hold. Using (30) and (33) with $Y_\pi = 1/Z_\pi$, (34) becomes

$$\begin{cases} V_1 = V_T \cosh k + I_T Z_0 \sinh k \\ I_1 = V_T \dfrac{\sinh k}{Z_0} + I_T \cosh k. \end{cases} \tag{35}$$

Now let us connect a second identical cell at its input and call V_2 and I_2 the voltage and the current at the input of the second cell. Similarly to (35)

$$\begin{cases} V_2 = V_1 \cosh k + I_1 Z_0 \sinh k \\ I_2 = V_1 \dfrac{\sinh k}{Z_0} + I_1 \cosh k \end{cases} \tag{36}$$

and substituting (35) in (36), we obtain

$$\begin{cases} V_2 = V_T \cosh 2k + I_T Z_0 \sinh 2k \\ I_2 = V_T \dfrac{\sinh 2k}{Z_0} + I_T \cosh 2k. \end{cases} \tag{37}$$

Generalizing (37) for n cells

$$\begin{cases} V_n = V_T \cosh nk + I_T Z_0 \sinh nk \\ I_n = V_T \dfrac{\sinh nk}{Z_0} + I_T \cosh nk. \end{cases} \tag{38}$$

Putting a terminating impedance $Z_T = V_T/I_T$ at the end of the line and calculating the ratio between the first and the second of (38) yields (3).

Furthermore, dividing the second of (38) by I_T yields the useful relation

$$\frac{I_T}{I_n} = \frac{1}{\frac{Z_T}{Z_0}\sinh nk + \cosh nk}. \tag{39}$$

Appendix II

A. Impedance of an n-Cell Resistive Line at Low Frequency

Consider the cascade of n cells of the type shown in Fig. 3(a), short circuited at the far end. The impedance of such line is given by (5) and (2). Let us develop the hyperbolic tangent term in (2)

$$\begin{aligned} \tanh nk &= \tanh n \cosh^{-1}\left(1 + \tfrac{1}{2}\,s\tau_w\right) \\ &= \tanh \ln\left[1 + \tfrac{1}{2}\,s\tau_w + \sqrt{\left(1 + \tfrac{1}{4}\,s\tau_w\right)^2 - 1}\right]^n \\ &= \frac{(1+x)^n - (1+x)^{-n}}{(1+x)^n + (1+x)^{-n}} \end{aligned} \tag{40}$$

where

$$x = \tfrac{1}{2}\,s\tau_w + \sqrt{s\tau_w\left(1 + \tfrac{1}{4}\,s\tau_w\right)}. \tag{41}$$

Expanding terms $(1+x)^n$ and $(1+x)^{-n}$ in (40) yields

$$\tanh nk \approx \frac{nx}{1 + \frac{1}{2}\,n^2x^2}. \tag{42}$$

Putting $s = j\omega$ in (41) and assuming suitably low frequencies

$$\omega \ll 1/\tau_w \tag{43}$$

(41) yields

$$x \approx \sqrt{s\tau_w\left(1 + \tfrac{1}{4}\,s\tau_w\right)}. \tag{44}$$

Substituting (44) in (42) yields

$$\tanh nk \approx \frac{n\sqrt{s\tau_w\left(1+\frac{1}{4}s\tau_w\right)}}{1+\frac{1}{2}n^2 s\tau_w\left(1+\frac{1}{4}s\tau_w\right)}. \tag{45}$$

Substituting (45) and (2) in (5) yields the low-frequency impedance Z_n of the n-cell line or

$$Y_n = \frac{1}{Z_n} \approx \frac{1}{nR} + \frac{nsC_w}{2}. \tag{46}$$

This is the parallel connection of an equivalent resistor nR and an equivalent capacitor $(1/2)nC_w$. Equation (46) is an acceptable approximation. In fact, the processing time must be greater than (12), which yields (43).

B. Impedance of an n-Cell Capacitive Line

Consider the cascade of n cells of the type shown in Fig. 3(b), short circuited at the far end. The impedance of such line is given by (5) and (2). A procedure similar to that of Appendix II-A, where R is substituted with $1/sC$ can be used to simplify (5). Instead of (43), we thus pose

$$\frac{C}{C_w} \gg 1 \tag{47}$$

and we finally get

$$Y_n = \frac{1}{Z_n} \approx \frac{sC}{n} + \frac{nsC_w}{2}. \tag{48}$$

The line impedance as expected is a pure capacitance, but two simple contributions are now put into evidence. Equation (48) is an acceptable approximation. In fact, (13) yields (47).

APPENDIX III
EQUIVALENT CIRCUIT FOR NOISE CALCULATIONS

Consider the circuit of Fig. 15, in which $Z_F = 1/Y_F$ is the impedance of a capacitance C_F in parallel with a resistor R_F

$$\frac{1}{Z_F} = Y_F = sC_F + \frac{1}{R_F} \tag{49}$$

and e_n, i_n are the instantaneous voltage and current noises. Let us propagate e_n and i_n to the output

$$V_{o1} = e_n \frac{\frac{1}{R_F} + \frac{1}{nR} + s(C_x + C_F)}{Y_n}$$
$$V_{o2} = -i_n \frac{1}{Y_n}. \tag{50}$$

V_{o1} and V_{o2} are the individual contributions of e_n and i_n to the output. C_x is the capacitive component of the input impedance. We now want to refer the first of (50) to an equivalent input current. To this purpose, we equal the first of (50) to the second, where i_n is substituted with the wanted equivalent current $i_{\rm eq}$. This yields

$$i_{\rm eq} = -e_n\left(\frac{1}{R_F} + \frac{1}{nR}\right) - e_n sC_t. \tag{51}$$

The overall equivalent noise current i_T flown into the amplifier virtual earth is so

$$i_T = i_n - e_n\left(\frac{1}{R_F} + \frac{1}{nR}\right) - e_n sC_t = i_n - i_{en} - e_n sC_t. \tag{52}$$

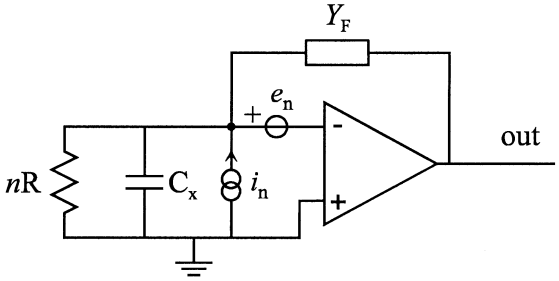

Fig. 15. Circuit for noise analysis.

Equation (52) shows that the principal system noises may be referred to the input by means of a unique noise current source injecting noise into the amplifier virtual earth. Equation (52) contains a term $e_n sC_t$ that can be conveniently visualized as a voltage source e_n injecting a current into the amplifier virtual earth through a capacitor $C_t = C_x + C_F$. The other components of the current noise source (52) have spectral densities (bilateral)

$$\frac{\overline{i_n^2}}{\delta f} = \frac{2KT}{nR} + \frac{2KT}{R_F} \tag{53}$$

$$\frac{\overline{i_{en}^2}}{\delta f} = 2KTR_S\left(\frac{1}{R_F} + \frac{1}{nR}\right)^2 \tag{54}$$

where R_S, or the series-noise equivalent resistor, is discussed after (17). It can be shown that (53) dominates over (54) if

$$R_S < \frac{nRR_F}{nR + R_F} \tag{55}$$

which is largely met in most cases, being R_S a few tens of ohms typically. We conclude that (52) yields in good approximation

$$i_T \approx i_n - e_n sC_t \tag{56}$$

or the sum of two uncorrelated components. Note that the sign "$-$" in (56) is not important, being e_n and i_n uncorrelated. Equation (56) is visualized by means of an equivalent circuit of the type of those shown in Fig. 10.

ACKNOWLEDGMENT

The authors would like to thank E. Gatti, P. Rehak, and I. Iori for fruitful discussions.

REFERENCES

[1] V. Radeka, "Position sensitive semiconductor detectors signal formation, noise and position readout," in *Proc. Workshop on Silicon Detectors for High Energy Physics Fexmilab*, Oct. 15–16, 1981, p. 21.
[2] R. B. Owen and M. L. Awcock, "One and two dimensional position sensing semiconductor detectors," *IEEE Trans. Nucl. Sci.*, vol. NS-15, pp. 290–303, Apr. 1968.
[3] A. Ghizzettti, *Calcolo Simbolico*. Bologna, Italy: Zanichelli, 1943, pp. 239–242.
[4] A. Van Der Ziel, "Noise in solid-state devices and lasers," *Proc. IEEE*, vol. 58, pp. 1178–1206, Aug. 1970.
[5] P. F. Manfredi, "New perspectives in low noise preamplifier design for room temperature X-ray detectors," in *Proc. Material Research Society Spring Meeting*, San Francisco, CA, Apr. 12–16, 1993, pp. 213–223.
[6] A. F. S. Goulding, "Pulse shaping in low-noise nuclear amplifiers: A physical approach to noise analysis," *Nucl. Instrum. Methods*, vol. 100, pp. 493–504, 1972.
[7] V. Radeka, "Optimum signal processing for pulse-amplitude spectrometry in the presence of high-rate effects and noise," *IEEE Trans. Nucl. Sci.*, vol. NS-15, pp. 455–481, June 1968.
[8] A. E. Gatti *et al.*, "Suboptimal filtering of $1/f$-noise in detector charge measurements," *Nucl. Instrum. Methods*, vol. A297, pp. 467–478, 1990.